INORGANIC CHEMISTRY FRONTIERS

RESEARCH ARTICLE

View Article Online
View Journal | View Issue

Cite this: *Inorg. Chem. Front.*, 2025, **12**, 7628

Siloxane-linked tungsten complexes form a flexible metal–organic framework: 1-D channel structure and gas adsorption property†

Ryo Nakamura,[a] Koichi Nagata,[a] Takahiro Kawatsu,[b] Kazuhiro Matsumoto,*[b] Yumiko Nakajima,[b] Takuji Ikeda,[c] Shinya Takaishi,[d] Wataru Kosaka,[e] Hitoshi Miyasaka[e] and Hisako Hashimoto*[a]

Received 20th May 2025,
Accepted 4th July 2025

DOI: 10.1039/d5qi01162k

rsc.li/frontiers-inorganic

Siloxane-linked tungsten complexes were synthesised by reacting a spiro-siloxane with tungsten(methyl) complexes, and they feature covalent W–Si/W=Si bonds coordinated by pyridine derivatives. Among these, $[Cp^*(OC)_2(Ph)W{=}Si(dmap)]_2$(spiro) (**4**) (dmap = 4-dimethylaminopyridine, spiro = spiro-siloxane) formed a porous framework with a 1-D channel structure in the crystalline state through CH–π interactions, as evaluated by single-crystal X-ray diffraction (SC-XRD) analysis. Powder X-ray diffraction (PXRD) analysis revealed that the structure of **4** reversibly changes upon the release and uptake of solvent molecules. Notably, the micro-ED measurement of the desolvated framework demonstrated a change in the space group and up to 14% contraction of its *b* axis, supporting the transformation of its geometrical features. Furthermore, gas adsorption measurements revealed that this framework exhibited gate-opening behavior toward gaseous molecules (5 and 4 mol mol^{-1} for CH_4 and O_2, respectively), highlighting the flexibility of the framework.

Introduction

Metal–organic frameworks (MOFs) represent a pivotal class in recent materials science, recognized for their high potential in various applications, attributable to their regulated porous structures.[1–3] Since the early 2000s, increasing attention has been directed toward a subclass of flexible MOFs, referred to as soft-porous crystals (SPCs), which exhibit reversible structural transformations of the pore size and shape, triggered by external factors such as temperature, pressure or guest molecule adsorption.[4–9] These properties are highly suitable for advanced gas separation, sensing and switchable catalysis. Such flexibility in MOFs can be achieved by carefully designing the coordination environment of metal nodes and selecting appropriate organic linkers. For instance, it has been reported that the incorporation of flexible aliphatic units into the linkers of frameworks induces a 'breathing behaviour', enabling reversible structural changes in response to the presence or absence of polar guest molecules.[10,11] It has also been found that linkers bearing hydroxy, amino or amide groups, among others, enable flexible frameworks through the formation of hydrogen bonds or π–π/CH–π interactions. These frameworks exhibit reversible crystal-to-crystal transformations upon the uptake and release of molecules.[12–15] More recently, the synthesis of frameworks with a catenated backbone has been reported, enabling switching between rigid and elastic states.[16] These examples illustrate promising strategies for accessing various types of flexible MOFs. However, achieving high-performance MOFs that exhibit both excellent flexibility and stability remains a significant challenge.

As stable and flexible linker units, we focused our attention on siloxanes. Siloxanes, which contain Si–O–Si bonds, are widely used as silicones in various industrial applications, including silicone oil, silicone rubber and medicinal ingredients.[17,18] Their versatility comes from their thermal and chemical stability, as well as their flexibility. The bond energy of the Si–O bond (549 kJ mol^{-1}) provides stability, while the

[a]*Inorganic Chemistry Laboratory, Department of Chemistry, Graduate School of Science, Tohoku University, Sendai, Miyagi, 980-8578, Japan. E-mail: hisako.hashimoto.b7@tohoku.ac.jp*
[b]*Interdisciplinary Research Center for Catalytic Chemistry (IRC3), National Institute of Advanced Industrial Science and Technology (AIST), Tsukuba, Ibaraki, 305-8565, Japan*
[c]*Research Institute for Chemical Process Technology, National Institute of Advanced Industrial Science and Technology (AIST), Sendai, Miyagi, 983-8551, Japan*
[d]*Coordination Chemistry Laboratory, Department of Chemistry, Graduate School of Science, Tohoku University, Sendai, Miyagi, 980-8578, Japan*
[e]*Institute for Materials Research, Tohoku University, Sendai, Miyagi, 980-8577, Japan*

†Electronic supplementary information (ESI) available: Synthetic and experimental procedures, characterisation data, details of X-ray crystallographic analysis, powder X-ray diffraction, micro-ED, thermogravimetric analysis, Le Bail analysis, gas sorption measurement and NMR spectra. CCDC 2445984 (**4**). For ESI and crystallographic data in CIF or other electronic format see DOI: https://doi.org/10.1039/d5qi01162k

wide range of Si–O–Si bond angles (130°–180°) imparts flexibility, making them more flexible than organic compounds with a carbon-based skeleton.[19] Porous materials incorporating such siloxane linkers are of great interest due to their potential achievement of flexibility. However, there have been only a few reports on the use of siloxane moieties incorporated in linkers in framework design. Davies *et al.* have reported the synthesis of frameworks with carboxylates containing siloxane moieties as linkers and their adsorption properties.[20] Their products exhibited superior hydrophobicity and water stability, although the flexibility of the frameworks is not referred to. Cazacu *et al.* synthesized MOFs using a siloxane-spaced dicarboxylic acid, which became amorphous while exhibiting hydrophobicity and a slightly lower glass transition temperature, just below room temperature.[21]

In this study, we aimed to incorporate an inherently flexible siloxane linker to impart flexibility to the framework. By focusing on spiro-type siloxanes with conformational regulation, we also envisaged to facilitate crystallisation of the framework and to gain access to detailed structural information. Moreover, to achieve enhanced thermal stability, we opted for covalent bonds instead of coordination bonds to connect the metal units and linkers, by applying a one-pot synthesis to obtain metal–silicon bonded complexes. Also, previous studies including ours[22] have demonstrated that the use of the oxidative addition/reductive elimination sequence between a labile methyl complex and hydrosilanes affords a silyl-type complex (**I**) and/or a silylene-type complex (**II**) (Scheme 1). This method is considered to produce a 16-electron intermediate (**a**), which facilitates the formation of silyl-type complex **I** *via* coordination of ligand L (Lewis base) to the metal. Meanwhile, silylene-type complex **II** is generated *via* a 1,2-group migration (**a** → **b**), followed by the coordination of L to the silicon atom. We anticipate that the transformability between the two forms, **I** and **II**, could also pave the way for molecular activation in future applications of this system.

We herein report the synthesis and isolation of several di-tungsten complexes linked with spiro-siloxane. Single-crystal X-ray diffraction (SC-XRD) analysis revealed that the compound bearing 4-dimethylaminopyridine (dmap) formed a 1-D channel structure in the crystalline state. Gas adsorption measurements and micro-ED analysis under desolvation conditions demonstrated that this framework was flexible.

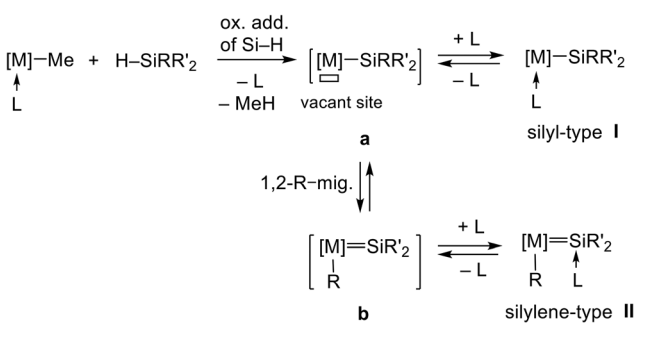

Scheme 1 Strategy for forming M–Si bonds. [M] = Cp*M(CO)$_n$, L = labile ligand (pyridine, DMAP, *etc.*), R, R′ = H, alkyl, aryl, *etc.*

Results and discussion

Syntheses of siloxane-linked di-tungsten complexes

Initially, we performed the reaction of Cp*W(CO)$_2$(py)Me (py = pyridine) with spiro-siloxane [H(Ph)Si{OSi(Me$_2$)O}$_2$]$_2$Si (**1**)[23] in a 2 : 1 ratio at room temperature for 2 h, which successfully afforded the siloxane-linked di-tungsten complex [Cp*(OC)$_2$(Ph)W=Si(py)]$_2$(spiro) (**2**) {spiro = –(OSiMe$_2$O)$_2$Si(OSiMe$_2$O)$_2$–} in a relatively high NMR yield (75%) (Scheme 2). During the reaction, an intermediate attributed to a mono-tungsten complex with the siloxane unit was observed by ^{1}H NMR, but it was cleanly converted into **2** in the final stage. Complex **2** was isolated in the pure form in 20% yield; the rather lower yield of **2** is due to its isomerisation to [Cp*(OC)$_2$(py)W–Si(Ph)]$_2$(spiro) (**3**) during purification. Thus, the isolated complex **2** gradually isomerised to yield **3** in 77% NMR yield, accompanied by 1,2-migration of the pyridine (from silicon to tungsten) and phenyl groups (from tungsten to silicon). Complex **3** was isolated in 34% yield based on **1** after recrystallization. Complex **2** was characterised as a base-stabilised silylene-type complex, whereas complex **3** was characterised as a silyl-type complex, based on multiple NMR measurements and the similarity of the NMR spectral data to those of the dmap analogue, [Cp*(OC)$_2$(Ph)W=Si(dmap)]$_2$(-spiro) (**4**), whose structure was confirmed by SC-XRD (*vide infra*). The di-nuclear compositions of **2** and **3** were confirmed by high-resolution mass spectrometry (HRMS), which revealed distinct molecular ion peaks.

In the ^{29}Si{^{1}H} NMR spectrum, complex **2** exhibited a signal of the silicon atom bonded to the tungsten atom at 27.0 ppm, with a satellite of tungsten ($^1J_{WSi}$ = 131 Hz, ^{183}W, nuclear spin = 1/2) (Table 1). This signal is considerably shifted downfield compared to that of the precursor spiro-siloxane **1** (−47.1 ppm), consistent with the formation of W–Si bonds. The satellite coupling constant $^1J_{WSi}$ also provides useful information about the bonding nature; the spin–spin coupling constant J reflects the s character of the nuclei involved in the bond.[24] Thus, the $^1J_{WSi}$ value (131 Hz) of **2** is close to that of the previously reported complex [Cp*(OC)$_2$(Me)W=Si(OMe)$_2$(dmap)] (**A**) ($^1J_{WSi}$ = 148 Hz),[25] suggesting the considerable sp^2 character of the Si atom involved in the W–Si bonds in **2**. In contrast, the $^1J_{WSi}$ value (53.8 Hz) of **3** at 21.5 ppm is much smaller than that of **2** and comparable to that of the related silyl complex [Cp*(OC)$_2$(dmap)W–SiMe$_2$Ph] (**B**) ($^1J_{WSi}$ = 31 Hz),[26] suggesting the sp^3-character of the Si atom bonded to tungsten in **3**. In addition, this type of isomerization from a silylene-type complex to a silyl complex has been previously found by our group; [Cp*(OC)$_2$(Ph)W=SiMe$_2$(dmap)] (**C**) was converted into **B** *via* 1,2-migration of the phenyl group.[26]

Next, we envisaged to obtain more stable products by replacing the coordinated pyridine with DMAP, which has more basicity and stronger coordination ability than pyridine {pK_a of

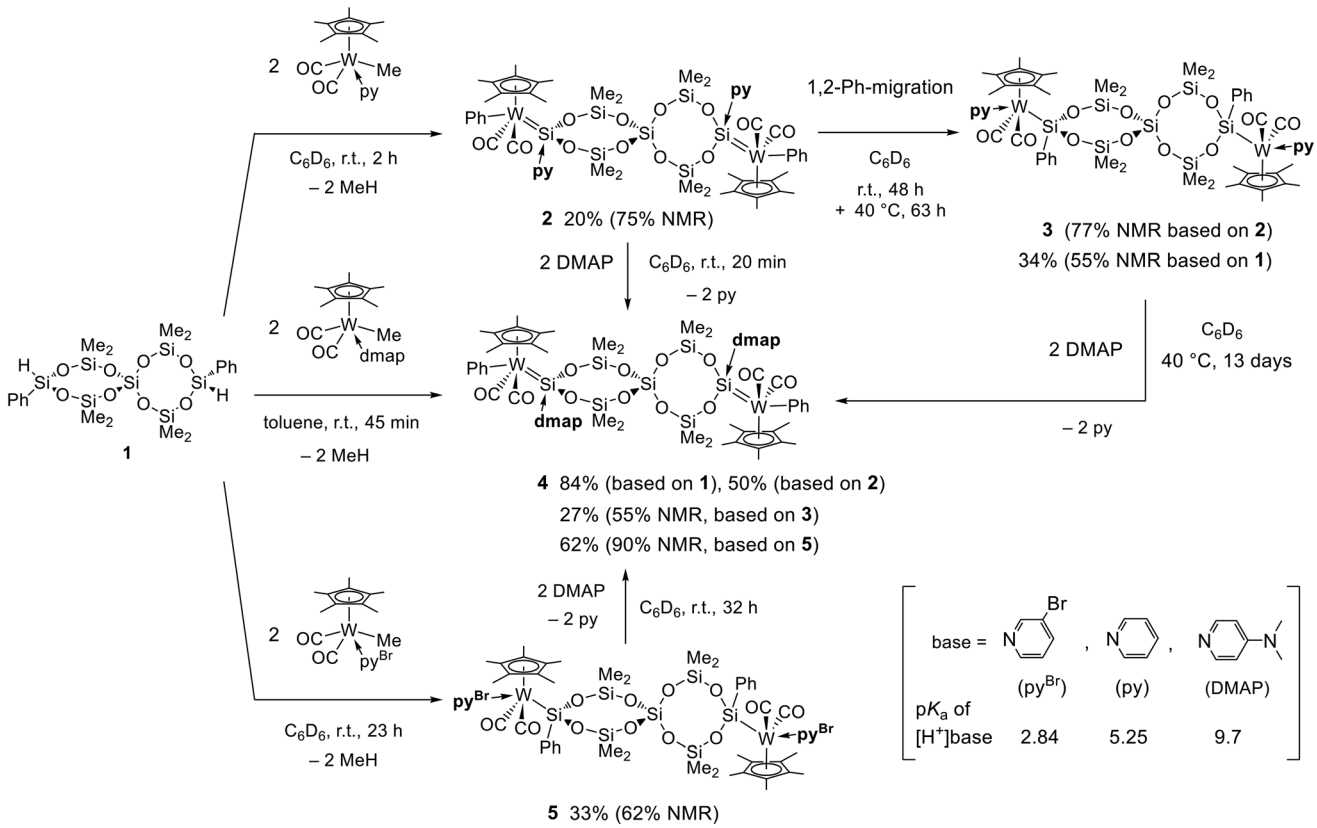

Scheme 2 Synthesis of **2–5** and pK_a of [H$^+$]base.[27]

Table 1 Selected ^{29}Si{^{1}H} NMR data of complexes **1–5**, **A** and **B** (SiH or SiW signals)

Complex	^{29}Si{^{1}H} NMR[a] (ppm)	$^1J_{WSi}$ (Hz)
[H(Ph)Si{OSi(Me$_2$)O}$_2$]$_2$Si (**1**)	−47.1 (SiH)	—
[Cp*(OC)$_2$(Ph)W=Si(py)]$_2$(spiro) (**2**)	27.0	131
[Cp*(OC)$_2$(py)W–Si(Ph)]$_2$(spiro) (**3**)	21.5	53.8
[Cp*(OC)$_2$(Ph)W=Si(dmap)]$_2$(spiro) (**4**)	22.8[b]	121
[Cp*(OC)$_2$(py^{Br})W–Si(Ph)]$_2$(spiro) (**5**)	21.1	53.3
[Cp*(OC)$_2$(Me)W=Si(OMe)$_2$(dmap)] (**A**)[c]	56.6	148
[Cp*(OC)$_2$(dmap)W–SiMe$_2$Ph] (**B**)[d]	15.8	31

[a] In C_6D_6. [b] In CD_2Cl_2. [c] From ref. 25. [d] From ref. 26.

[H$^+$]base: 5.25 (H$^+$·py) < 9.7 (H$^+$·DMAP)}.[27] As expected, the addition of DMAP to complex **2** resulted in a facile exchange of pyridine with DMAP to produce [Cp*(OC)$_2$(Ph)W=Si(dmap)]$_2$(spiro) (**4**) (Scheme 2). The pyridine/DMAP exchange also proceeded from **3** to give **4**, accompanied by 1,2-Ph migration. Consequently, **4** was more directly obtained by the reaction of the dmap-methyl complex Cp*W(CO)$_2$(dmap)Me[26] and spiro-siloxane **1**, from which **4** was isolated in the highest yield (84%). The ^{29}Si{^{1}H} NMR of **4** exhibits a signal at 22.8 ppm with a relatively large $^1J_{WSi}$ coupling of 121 Hz, suggesting that **4** is a base-stabilised silylene complex (Table 1); this value is larger than that of the silyl complex **3** ($^1J_{WSi}$ = 53.8 Hz) but is close to those of silylene-type complexes **A** ($^1J_{WSi}$ = 148 Hz) and **2** ($^1J_{WSi}$ = 131 Hz). On the other hand, we also tested the reaction of **1** with a more labile methyl complex with a much weaker coordination ligand {py^{Br} = 3-bromopyridine, pK_a of [H$^+$]base: 2.84 (H$^+$·py^{Br}) < 5.25 (H$^+$·py)},[27a] as a starting precursor. Thus, the reaction of Cp*W(CO)$_2$(py^{Br})Me with **1** gave solely silyl complex **5** in a much shorter reaction time (compared with the formation of **3**) (Scheme 2). The ^{29}Si{^{1}H} NMR signal data (21.1 ppm, $^1J_{WSi}$ = 53.3 Hz) agree with the observation that **5** is a silyl-type complex (Table 1): there was no observation of a silylene-type complex. Complex **5** was efficiently converted into **4** by the reaction with DMAP (90% NMR yield) due to its facile substitution ability.

Solid-state molecular structure of the tungsten di-nuclear complex 4

SC-XRD analysis clearly revealed that **4** is a di-nuclear complex bridged by a spiro-siloxane moiety (Fig. 1). Each tungsten centre of **4** adopts a four-legged piano-stool geometry, with the nitrogen atom N1 of the dmap being coordinated to the silicon atom Si1. The W–Si bond lengths [2.465(5), 2.470(6) Å] are within the range of those of base-stabilised tungsten(silylene) complexes (2.45–2.51 Å).[28] The Si–N bond lengths [1.880 (13), 1.86(2) Å] are longer than the usual Si–N covalent bond lengths (1.70–1.76 Å),[29] suggesting the coordination character of these bonds. These lengths are slightly shorter than those

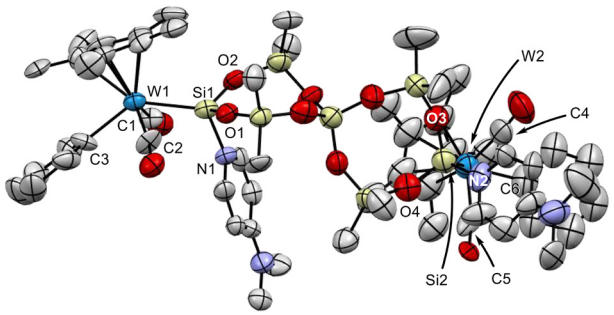

Fig. 1 Crystal structure of $[Cp^*(OC)_2(Ph)W{=}Si(dmap)]_2$(spiro) (**4**). Selected interatomic distances (Å): W(1)–Si(1) 2.465(5), Si(1)–N(1) 1.880 (13), W(2)–Si(2) 2.470(6), Si(2)–N(2) 1.86(2). Hydrogen atoms and crystal solvents are omitted for clarity.

of the reported nitrogen-coordinated silylene complexes [1.908 (2)–2.007(9) Å],[30] implying rather stronger coordination of dmap in **4**. The sums of the three bond angles around the Si atoms [344.4(7)°, 343.7(8)°], excluding the Si–N bonds, are intermediate between those of the ideal tetrahedral geometry (329°) for sp^3-Si and the trigonal planar geometry (360°) for sp^2-Si. All these features are characteristics of a base-stabilised silylene complex and indicate the relatively strong coordination of dmap to the silylene moiety.

Packing structure of complex 4

The packing structures of complex **4** are illustrated in Fig. 2a–c, along the *a*-, *b*- and *c*-axis directions. It is clearly observed from these figures that the complex forms a porous 1-D channel structure along the *c*-axis direction. The pore size is about 9 Å × 18 Å (Fig. 2d and e). The pores contain CH_2Cl_2 and THF as the crystal solvents, but their positions were not determined due to their random arrangement. The view focusing on the area around dmap ligands (Fig. 3) shows the existence of two types of CH–π intermolecular interactions in the crystalline state: (i) CH–π(py) interaction between the hydrogen atoms of the (dimethyl)amino groups of dmap ligands and the carbon atoms at the 3-position of the six-membered rings, (ii) CH–π(CO) interaction between the hydrogen atoms of the (dimethyl)amino groups and the carbon atoms of the CO ligands. The distances between these atoms are (i) 2.86 Å and (ii) 2.63 Å, respectively, which are within the range of the CH–π interaction length (2.6–3.0 Å).[31] These multiple interactions appear to play a role in shaping the framework.

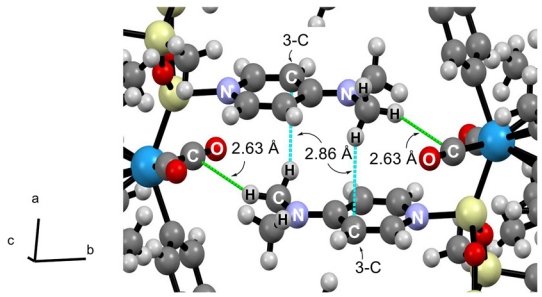

Fig. 3 CH–π interaction in the crystal of **4** around the dmap ligands: atomic codes W, light blue; C, grey; N, purple; O, red; Si, light yellow; and H, white. Blue line: CH–π(py), green line: CH–π(CO) interaction.

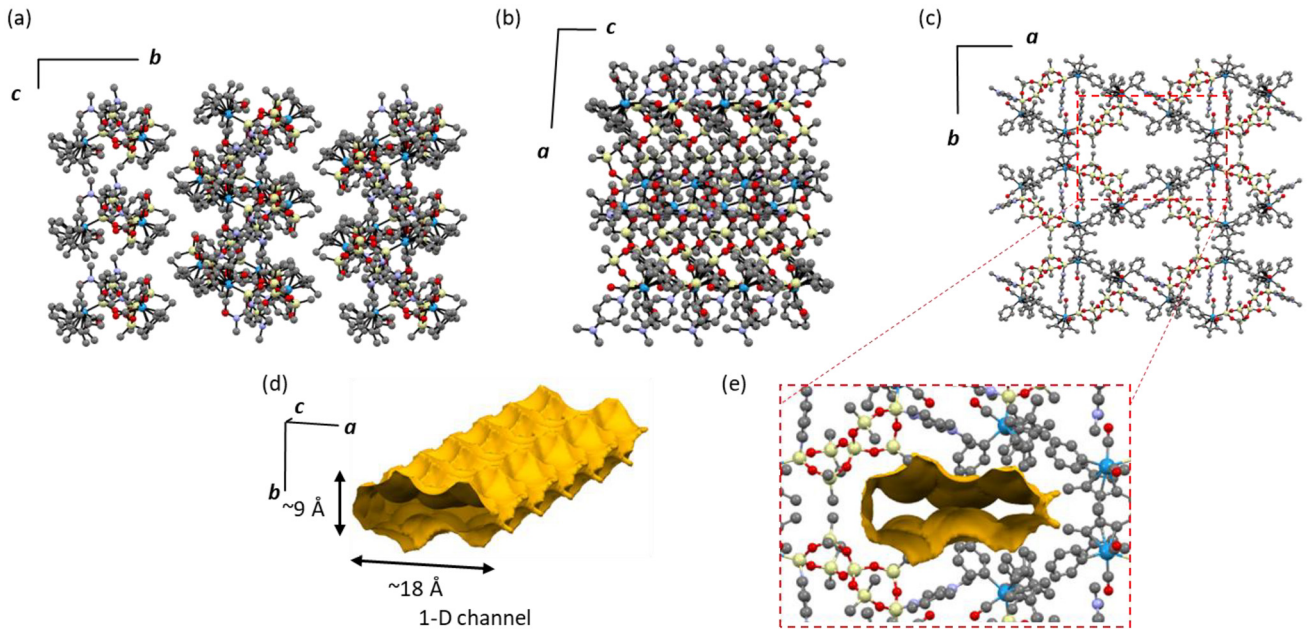

Fig. 2 Packing structure of $[Cp^*(OC)_2(Ph)W{=}Si(dmap)]_2$(spiro) (**4**), along the (a) *a*-, (b) *b*- and (c) *c*-axis: atomic codes W, light blue; C, grey; N, purple; O, red; and Si, light yellow. Hydrogen atoms and crystal solvents are omitted for clarity. (d) View of the 1-D channel in the crystal phase of **4**. (e) Enlarged view of the pore along the *c*-axis.

Uptake of solvent molecules by complex 4

The presence of the 1-D channel structure in **4** encouraged us to investigate the adsorption property of **4** in the solid state.[12,16] The powder X-ray diffraction (PXRD) pattern of the samples A–E and the simulation pattern I obtained from the SC-XRD analysis of **4** are shown in Fig. 4 (see the ESI, Fig. S2†). The PXRD pattern II of sample A, which is a crystal of the mother liquor, is consistent with simulation I. The PXRD pattern III of sample B, which is a powder of **4** obtained after drying under reduced pressure, differs significantly from simulation I. This observation suggests that **4** was transformed into a different framework from that of the single-crystal structure upon drying.

Pattern III is essentially identical to pattern IV of sample C, which is crystals dried slowly under Ar, suggesting that the drying speed has no impact on this structural transformation. Moreover, this characteristic implies the ease with which the crystalline solvent can be desolvated and activated, making it highly suitable for application as a gas adsorption material. In pattern V of sample D, which consisted of dried powder B immersed in *n*-hexane at room temperature, superimposed features of the patterns of samples A and B were observed. These results demonstrate that immersing the dried powder of complex **4** (sample B) in *n*-hexane enables the solvents to penetrate the pores, gradually reconstructing the original 1-D channel structure. This process is identified as a solid-to-solid transition, rather than recrystallisation, due to the insolubility of **4** in *n*-hexane. Furthermore, a comparison between pattern VI of sample E, which is dried powder B immersed in *n*-hexane at room temperature for 47 days, and pattern V of sample D, immersed for 19 days, clearly reveals that the component corresponding to sample A increased in sample E. This result indicates that extended immersion in *n*-hexane leads to an increased proportion of 1-D channel structures.

Based on these observations from the PXRD patterns of samples A, B, D and E, it is evident that **4** undergoes a reversible framework transformation upon the release and uptake of solvent molecules (*n*-hexane). In addition, attempts were made to perform SC-XRD measurement on the dried structure; however, the detailed structure could not be determined due to its small crystalline size.

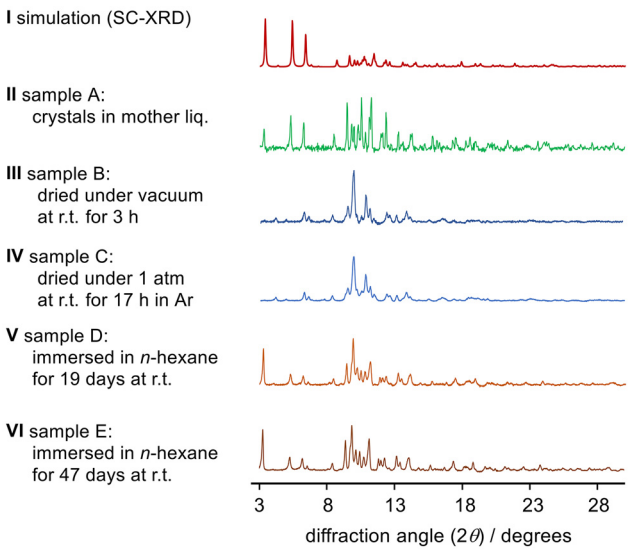

Fig. 4 Powder X-ray diffraction patterns of **4**. I: the simulation pattern obtained from the SC-XRD analysis; II: the PXRD pattern of sample A – crystals in mother liq.; III: sample B – dried under vacuum; IV: sample C – dried under Ar; V: sample D – immersed in *n*-hexane for 19 days at r.t.; and VI: sample E – immersed in *n*-hexane for 47 days at r.t. (2θ = 3–30°).

Micro-ED measurements of dried complex 4

To gain further insight into the dried structure of complex **4** (dried-**4**), we conducted micro-ED analysis, which revealed the lattice parameters of dried-**4**, although the molecular structure of dried-**4** was not determined. Surprisingly, upon desolvation, the space group transformed from $P2_1/c$ to $P\bar{1}$ (or $P1$), accompanied by a reduction in the *b*-axis unit cell from approximately 33 Å to 28 Å, representing a 14% decrease (Table 2). Along with the reduction of the *b*-axis, the cell volume decreased from approximately 8128 Å^3 to 7056 Å^3, representing 13% shrinkage. It is important to note that using the lattice constants obtained from micro-ED analysis, the observed PXRD pattern was well fitted by the Le Bail method (Fig. S6†), indicating that the obtained powder is a single-phase. The slight difference between the lattice constants refined by the Le Bail analysis and those obtained by micro-ED may be due to the difference in measurement conditions; micro-ED measurements were carried out under vacuum conditions, while the PXRD was performed under atmospheric pressure.

Gas adsorption measurements of complex 4

PXRD analysis demonstrated the capability of the framework to incorporate molecules into its pores, suggesting its potential application in gas adsorption. Accordingly, gas adsorption measurements were conducted on powder samples of complex **4** for CO_2 (195 K), CH_4 (112 K), O_2 (90 K), N_2 (77 K or 120 K), Ar (87 K) and H_2 (77 K). As shown in the adsorption isotherm of CO_2 gas in Fig. 5, two molecules of CO_2 were adsorbed per formula unit of complex **4** (equivalent to 27.4 cm^3 g^{-1} at standard temperature and pressure) and the adsorption isotherm illustrated a slightly stepwise adsorption behavior. However,

Table 2 Unit cell parameters of complex **4** (SC-XRD) and dried-**4** (micro-ED)

	4	Dried-**4**
Crystal system	Monoclinic	Triclinic
Space group	$P2_1/c$	$P\bar{1}$ (or $P1$)
a [Å]	26.0217(13)	26.737(11)
b [Å]	32.6729(15)	28.087(8)
c [Å]	9.5848(4)	9.577(3)
α [°]	90	95.94(3)
β [°]	94.109(4)	91.77(4)
γ [°]	90	99.01(3)
V [Å^3]	8128.1(6)	7056(4)

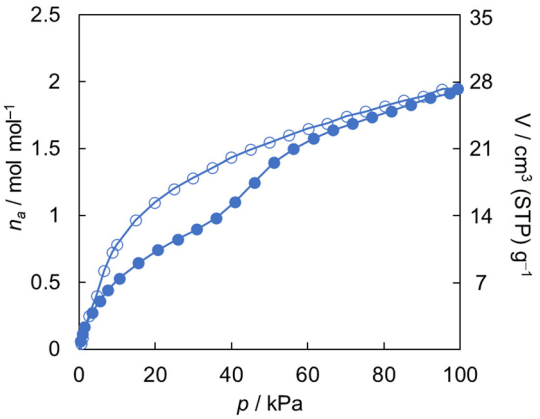

Fig. 5 Adsorption isotherm of CO_2 at 195 K. The solid and open circles in blue represent adsorption and desorption, respectively.

the sorption process did not induce any substantial structural changes in the framework, as evidenced by the *in situ* PXRD experiments conducted under a CO_2 atmosphere at 195 K (Fig. S8†). In contrast, the adsorption isotherms for CH_4 and O_2 exhibited distinct gate-opening behavior during the adsorption of these gases (Fig. 6). Gate-opening adsorption refers to the behavior in which gas molecules are absorbed, as the framework of the adsorbent undergoes a structural transition at a specific threshold gas pressure. This phenomenon can be attributed to the structural flexibility of the framework in response to guest stimuli.[1b,32] At 100 kPa, the CH_4 uptake at 112 K reached 5 mol mol^{-1} (69.7 cm^3 g^{-1} at STP) and the adsorption isotherm exhibited an abrupt increase at 77 kPa, along with pronounced hysteresis. In the O_2 isotherm at 90 K, the adsorption capacity was determined to be 4 mol mol^{-1} (55.9 cm^3 g^{-1} at STP), showing a gradual increase at 60–70 kPa and exhibiting pronounced hysteresis as well. In contrast, the adsorption of other gaseous molecules (N_2, Ar and H_2) was not observed (Fig. S7†). The minimal N_2 adsorption at 77 K can be attributed to the kinetic constraints, specifically the rigidity of the framework at low temperatures. This is supported by the slightly higher N_2 adsorption observed at 120 K (3.02 cm^3 g^{-1} at STP) than that at 77 K (1.73 cm^3 g^{-1} at STP). Similarly, the absence of Ar (87 K) and H_2 (77 K) uptake can be attributed to the kinetic constraints. Interestingly, however, clear adsorption behavior was observed for O_2 gas, despite its physical and electrical properties being similar to those of Ar. This phenomenon may be ascribed to the sensitivity of the framework to subtle variations in quadrupole moment or adsorption temperature, although the specific mechanisms remain unclear (Table S4†). Additionally, the ability of the framework to adsorb CH_4 suggests that its selectivity may also be influenced by the polarizability of guest molecules.

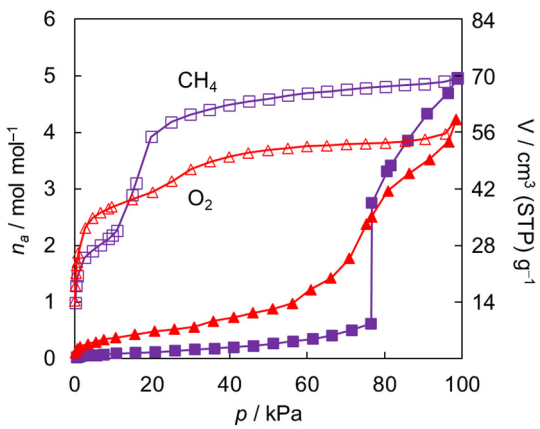

Fig. 6 Adsorption isotherms of CH_4 (112 K) and O_2 (90 K). The solid-open square and triangle represent the adsorption–desorption of CH_4 and O_2, respectively.

In general, the solid phase typically exists in its most stable conformation, and any conformational changes are energetically unfavorable.[33] Therefore, when gate-opening adsorption takes place, as observed in the present case, stabilisation must occur to offset the destabilisation caused by the conformational changes induced during adsorption. Hence, host–guest interaction that stabilises the guest-adsorbed phase is essential. The adsorption of CH_4 and O_2 is believed to involve interactions between the framework and these gases (CH_4 or O_2), arising from the polarisation of electric charge distribution or dielectric effects. These interactions likely drive the observed adsorption behavior. Whether this dynamic behavior stems from the introduction of the siloxane remains to be investigated. Our future studies will include determining the crystal structure of the dried phase, conducting spectroscopic measurements (IR and Raman) under gas atmospheres, and performing control experiments using a porous material lacking siloxane units. Additionally, it should be noted that this siloxane-based porous material has potential applications in gas separation and sensing due to its high adsorption selectivity for O_2 and CH_4 over other gases (N_2, Ar and H_2). Future research will also focus on adsorption measurements using gas mixtures and breakthrough curve analyses.

Conclusions

In summary, this study aimed to synthesise complexes linked by siloxanes to achieve flexible structures. Di-nuclear complexes **2–5** linked with siloxane were successfully synthesised, and their structures were elucidated by multiple spectroscopic techniques, along with SC-XRD analysis of **4**. The SC-XRD study confirmed that complex **4** is a di-nuclear complex featuring dmap-coordinated W═Si bonds, forming a porous framework with a 1-D channel structure in its crystalline state through intermolecular CH–π interactions. The PXRD analyses reveal that the dried powder of **4** reconstructs the 1-D channel structure upon immersion in *n*-hexane. Moreover, gas adsorption measurements revealed that the framework adsorbs two molecules of CO_2, four molecules of O_2, and five molecules of CH_4 per formula unit of **4**. Notably, only in the cases of CH_4 and O_2, does this compound exhibit sorption phenomena characteristic of gate-type sorption behavior, highlighting the

flexibility of the framework. This is further supported by micro-ED analysis, which demonstrated changes in the lattice parameters upon desolvation. This phenomenon is thought to result from the introduction of a flexible siloxane into the framework. Further investigations on the effect of the siloxane unit, adsorption behavior, and properties of other analogous complexes are in progress.

Author contributions

Conceptualisation, methodology, K. M., Y. N. and H. H.; synthesis, R. N., T. K.; analysis, investigation, validation, R. N., K. N., T. I., S. T., W. K., H. M.; resources, visualization, funding acquisition, K. N. and H. H.; original draft preparation, R. N.; review and editing, supervision, project administration, H. H. All authors have read and agreed to the published version of the manuscript.

Conflicts of interest

There are no conflicts to declare.

Data availability

The data supporting this article have been included in the ESI.† Synthetic and experimental procedures, characterisation data, details of X-ray crystallographic analysis, powder X-ray diffraction, micro-ED, thermogravimetric analysis, Le Bail analysis, gas sorption measurement and NMR spectra. The crystallographic data for the X-ray crystallographic coordinates of structures reported in this study have been deposited at the Cambridge Crystallographic Data Centre (CCDC) under deposition number CCDC 2445984.†

Acknowledgements

This work was supported by JSPS KAKENHI grants JP_ 15K05444, 22H02088, 23K23356 (HH), and 21K14638 (KN) from the Japan Society for the Promotion of Science (JSPS), and by JST SPRING, Grant Number JPMJSP2114 (RN). This work was supported by JST-FOREST (Fusion Oriented Research for Disruptive Science) (YN). We thank Mr H. Sato (Rigaku Corporation, Tokyo, Japan) for his support in XRD study and are also grateful to the Research and Analytical Center for Giant Molecules (Tohoku University) for mass and elemental analyses. The micro-ED analysis was supported by the Nanomaterial Evaluation and Prototyping Platform (NEPP) at AIST Tohoku.

References

1 (*a*) S. Kitagawa and M. Kondo, Functional Micropore Chemistry of Crystalline Metal Complex-Assembled Compounds, *Bull. Chem. Soc. Jpn.*, 1998, **71**, 1739–1753; (*b*) S. Kitagawa, R. Kitaura and S. Noro, Functional Porous Coordination Polymers, *Angew. Chem., Int. Ed.*, 2004, **43**, 2334–2375; (*c*) S. Kitagawa and R. Matsuda, Chemistry of coordination space of porous coordination polymers, *Coord. Chem. Rev.*, 2007, **251**, 2490–2509.

2 J.-R. Li, J. Sculley and H.-C. Zhou, Metal–Organic Frameworks for Separations, *Chem. Rev.*, 2012, **112**, 869–932.

3 H. Furukawa, K. E. Cordova, M. O'Keeffe and O. M. Yaghi, The Chemistry and Applications of Metal-Organic Frameworks, *Science*, 2013, **341**, 1230444.

4 G. Ferey and C. Serre, Large breathing effects in three-dimensional porous hybrid matter: facts, analyses, rules and consequences, *Chem. Soc. Rev.*, 2009, **38**, 1380–1399.

5 S. Horike, S. Shimomura and S. Kitagawa, Soft porous crystals, *Nat. Chem.*, 2009, **1**, 695–704.

6 M. Li, D. Li, M. O'Keeffe and O. M. Yaghi, Topological Analysis of Metal–Organic Frameworks with Polytopic Linkers and/or Multiple Building Units and the Minimal Transitivity Principle, *Chem. Rev.*, 2014, **114**, 1343–1370.

7 A. Schneemann, V. Bon, I. Schwedler, I. Senkovska, S. Kaskel and R. A. Fischer, Flexible metal–organic frameworks, *Chem. Soc. Rev.*, 2014, **43**, 6062–6096.

8 L. Sarkisov, R. L. Martin, M. Haranczyk and B. Smit, On the Flexibility of Metal–Organic Frameworks, *J. Am. Chem. Soc.*, 2014, **136**, 2228–2231.

9 R. Pallach, J. Keupp, K. Terlinden, L. F. Beyme, M. Kloß, A. Machalica, J. Kotschy, S. K. Vasa, P. A. Chater, C. Sternemann, M. T. Wharmby, R. Linser, R. Schmid and S. Henke, Frustrated flexibility in metal-organic frameworks, *Nat. Commun.*, 2021, **12**, 4097.

10 S. Henke, D. C. F. Wieland, M. Meilikhov, M. Paulus, C. Sternemann, K. Yusenko and R. A. Fischer, Multiple phase-transitions upon selective CO_2 adsorption in an alkyl ether functionalized metal–organic framework—an *in situ* X-ray diffraction study, *CrystEngComm*, 2011, **13**, 6399–6404.

11 H. Reinsch, R. S. Pillai, R. Siegel, J. Senker, A. Lieb, G. Maurin and N. Stock, Structure and properties of Al-MIL-53-ADP, a breathing MOF based on the aliphatic linker molecule adipic acid, *Dalton Trans.*, 2016, **45**, 4179–4186.

12 K. Uemura, S. Kitagawa, M. Kondo, K. Fukui, R. Kitaura, H.-C. Chang and T. Mizutani, Novel Flexible Frameworks of Porous Cobalt(II) Coordination Polymers That Show Selective Guest Adsorption Based on the Switching of Hydrogen-Bond Pairs of Amide Groups, *Chem. – Eur. J.*, 2002, **8**, 3587–3600.

13 N. Dissem, M. Essalhi, N. Ferhi, A. Abidi, T. Maris and A. Duong, Flexible and porous 2D layered structures based on mixed-linker metal–organic frameworks for gas sorption studies, *Dalton Trans.*, 2021, **50**, 8727–8735.

14 R. Kitaura, K. Seki, G. Akiyama and S. Kitagawa, Porous Coordination-Polymer Crystals with Gated Channels Specific for Supercritical Gases, *Angew. Chem., Int. Ed.*, 2003, **42**, 428–431.

15 K. Roztocki, W. Gromelska, F. Formalik, A. Giordana, L. Andreo, G. Mahmoudi, V. Bon, S. Kaskel, L. J. Barbour, A. Janiak and E. Priola, Shape-Memory Effect Triggered by (–(Interactions in a Flexible Terpyridine Metal–Organic Framework, *ACS Mater. Lett.*, 2023, **5**, 1256–1260.

16 W. Meng, S. Kondo, T. Ito, K. Komatsu, J. Pirillo, Y. Hijikata, Y. Ikuhara, T. Aida and H. Sato, An elastic metal–organic crystal with a densely catenated backbone, *Nature*, 2021, **598**, 298–303.

17 (*a*) E. G. Rochow, *Silicon and Silicones*, Springer-Verlag Berlin Heidelberg New York London Paris Tokyo, 1987; (*b*) J. Martín-Gil, F. J. Martín-Gil, A. I. De Andrés-Santos, M. C. Ramos-Sànchez, M. T. Barrio-Arredondo and N. Chebib-Abuchalà, Thermal behaviour of medical grade silicone oils, *J. Anal. Appl. Pyrolysis*, 1997, **42**, 151–158; (*c*) H. Miyahara, A. Nakajima, J. Wada and S. Yanabu, Breakdown Characteristics of Combined Insulation in Silicone Oil for Electric Power Apparatus, *2006 IEEE 8th International Conference on Properties and applications of Dielectric Materials*, 661–664; (*d*) R. H. Doremus, Viscosity of silica, *J. Appl. Phys.*, 2002, **92**, 7619–7629.

18 (*a*) M. Unno, A. Suto and T. Matsumoto, Laddersiloxanes—silsesquioxanes with defined ladder structure, *Russ. Chem. Rev.*, 2013, **82**, 289–302; (*b*) Y. Liu, T. Chaiprasert, A. Ouali and M. Unno, Well-defined cyclic silanol derivatives, *Dalton Trans.*, 2022, **51**, 4227–4245.

19 (*a*) M. A. Brook, *Silicon in Organic, Organometallic, and Polymer Chemistry*, John Wiley & Sons, New York, 2000; (*b*) F. Weinhold and R. West, The Nature of the Silicon–Oxygen Bond, *Organometallics*, 2011, **30**, 5815–5824.

20 (*a*) L. C. Delmas, A. J. P. White, D. Pugh, A. Evans, M. A. Isbell, J. Y. Y. Heng, P. D. Lickiss and R. P. Davies, Stable metal–organic frameworks with low water affinity built from methyl-siloxane linkers, *Chem. Commun.*, 2020, **56**, 7905–7908; (*b*) L. C. Delmas, P. N. Horton, A. J. P. White, S. J. Coles, P. D. Lickiss and R. P. Davies, Studies on the structural diversity of MOFs containing octahedral siloxane-backboned connectors, *Polyhedron*, 2019, **157**, 25–32; (*c*) L. C. Delmas, P. N. Horton, A. J. P. White, S. J. Coles, P. D. Lickiss and R. P. Davies, Siloxane-based linkers in the construction of hydrogen bonded assemblies and porous 3D MOFs, *Chem. Commun.*, 2017, **53**, 12524–12527.

21 M. Cazacu, G.-O. Turcan-Trofin, A. Vlad, A. Bele, S. Shova, A. Nicolescu and A. Bargan, Hydrophobic, amorphous metal–organic network readily prepared by complexing the aluminum ion with a siloxane spaced dicarboxylic acid in aqueous medium, *J. Appl. Polym. Sci.*, 2019, **136**, 47144.

22 (*a*) H. Sakaba, M. Tsukamoto, T. Hirata, C. Kabuto and H. Horino, Synthesis, Structure, and Silylene Exchange Reaction of Base-Stabilized Hydrido(silylene)tungsten Complexes and Rearrangement of Hydrosilyl(pyridine)tungsten Complexes to the Base-Stabilized Hydrido(silylene) Complexes via 1,2-Hydrogen Migration, *J. Am. Chem. Soc.*, 2000, **122**, 11511–11512; (*b*) K. Ueno, S. Asami, N. Watanabe and H. Ogino, Synthesis of Self-Stabilized and Donor-Free Silyl(silylene)tungsten Complexes, *Organometallics*, 2002, **21**, 1326–1328; (*c*) H. Tobita, A. Matsuda, H. Hashimoto, K. Ueno and H. Ogino, Direct Evidence for Extremely Facile 1,2- and 1,3-Group Migrations in an $FeSi_2$ System, *Angew. Chem., Int. Ed.*, 2004, **43**, 221–224.

23 T. Kawatsu, K. Fuchise, K. Takeuchi, J.-C. Choi, K. Sato and K. Matsumoto, Well-defined hydrogen and organofunctional polysiloxanes with spiro-fused siloxane backbones, *Polym. Chem.*, 2021, **12**, 2222–2227.

24 (*a*) N. F. Ramsey, Electron Coupled Interactions between Nuclear Spins in Molecules, *Phys. Rev.*, 1953, **91**, 303–307; (*b*) H. McConnell, Molecular Orbital Approximation to Electron–Spin Coupled Nuclear Spin–Spin Interactions in Molecules, *J. Chem. Phys.*, 1955, **27**, 760; (*c*) H. M. McConnell, Molecular Orbital Approximation to Electron Coupled Interaction between Nuclear Spins, *J. Chem. Phys.*, 1956, **24**, 460–467; (*d*) F. H. Köhler, H. J. Kalder and E. O. Fisher, Die Metall–Kohlenstoff-Bindung in Carben- und Carbin-Komplexen. Aussagen Der ^{183}W–^{13}C-Kopplungen, *J. Organomet. Chem.*, 1976, **113**, 11–22.

25 E. Suzuki, T. Komuro, Y. Kanno, M. Okazaki and H. Tobita, Facile 1,2-Migration of a Methyl Group on a {Dimethoxy(methyl)silyl}tungsten Complex: Formation of a Base-Stabilized (Dimethoxysilylene)(methyl) Complex, *Organometallics*, 2010, **29**, 5296–5300.

26 E. Suzuki, T. Komuro, M. Okazaki and H. Tobita, Synthesis and Characterization of DMAP-Stabilized Aryl(silylene) Complexes and (Arylsilyl)(DMAP) Complexes of Tungsten: Mechanistic Study on the Interconversion between These Complexes via 1,2-Aryl Migration, *Organometallics*, 2009, **28**, 1791–1799.

27 (*a*) J. R. Rumble, *CRC handbook of chemistry and physics*, 104th ed., CRC Press, Boca Raton, 2023; (*b*) C. T. Watson, S. Cai, N. V. Shokhirev and F. A. Walker, NMR and EPR Studies of Low-Spin Fe(III) Complexes of *meso*-Tetra-(2,6-Disubstituted Phenyl)Porphyrinates Complexed to Imidazoles and Pyridines of Widely Differing Basicities, *Inorg. Chem.*, 2005, **44**, 7468–7484.

28 M. Okazaki, E. Suzuki, N. Miyajima, H. Tobita and H. Ogino, Facile Isomerization of a Tungsten Silyl Complex to a Base-Stabilized Silylene Complex via 1,2-Migration of an Aryl Group, *Organometallics*, 2003, **22**, 4633–4635.

29 W. S. Sheldrick, *The Chemistry of Organic Silicon Compounds*, John Wiley & Sons, New York, 1989, Chapter 3.

30 M. Hirotsu, T. Nunokawa and K. Ueno, Synthesis and Reactivity of a Donor-Free (Silyl)(silylene)molybdenum Complex: Novel Insertion Reaction of an Isocyanide into a Si-C Bond, *Organometallics*, 2006, **25**, 1554–1556.

31 (*a*) C. Zhao, R. M. Parrish, M. D. Smith, P. J. Pellechia, C. D. Sherrill and K. D. Shimizu, Do Deuteriums Form Stronger CH–π Interactions?, *J. Am. Chem. Soc.*, 2012, **134**, 14306–14309; (*b*) M. Nishio, CH/π hydrogen bonds in crystals, *CrystEngComm*, 2004, **6**, 130–158; (*c*) M. Nishio, The CH/π hydrogen bond in chemistry. Conformation, supramolecules, optical resolution and interactions involving

carbohydrates, *Phys. Chem. Chem. Phys.*, 2011, **13**, 13873–13900; (*d*) M. Nishio, Y. Umezawa, J. Fantini, M. S. Weiss and P. Chakrabarti, CH–π hydrogen bonds in biological macromolecules, *Phys. Chem. Chem. Phys.*, 2014, **16**, 12648–12683; (*e*) M. Nishio, M. Hirota and Y. Umezawa, *The CH/π interaction evidence, nature, and consequence*, Wiley-VCH, New York, 1998, Chapter 6; (*f*) F. A. Perras, D. Marion, J. Boisbouvier, D. L. Bryce and M. J. Plevin, Observation of CH···π Interactions between Methyl and Carbonyl Groups in Proteins, *Angew. Chem., Int. Ed.*, 2017, **56**, 7564–7567.

32 (*a*) S. Shimomura, M. Higuchi, R. Matsuda, K. Yoneda, Y. Hijikata, Y. Kubota, Y. Mita, J. Kim, M. Takata and S. Kitagawa, Selective sorption of oxygen and nitric oxide by an electron-donating flexible porous coordination polymer, *Nat. Chem.*, 2010, **2**, 633–637; (*b*) S. Kusaka, Y. Itoh, A. Hori, J. Usuba, J. Pirillo, Y. Hijikata, Y. Ma and R. Matsuda, Adsorptive-dissolution of O_2 into the potential nanospace of a densely fluorinated metal-organic framework, *Nat. Commun.*, 2024, **15**, 10117.

33 (*a*) H. P. G. Thompson and G. M. Day, Which conformations make stable crystal structures? Mapping crystalline molecular geometries to the conformational energy landscape, *Chem. Sci.*, 2014, **5**, 3173–3182; (*b*) S. L. Price, Control and prediction of the organic solid state: a challenge to theory and experiment, *Proc. R. Soc. Ser. A*, 2018, **474**, 20180351; (*c*) S. E. Wright, J. C. Cole and A. J. Cruz-Cabeza, Conformational Change in Molecular Crystals: Impact of Solvate Formation and Importance of Conformational Free Energies, *Cryst. Growth Des.*, 2021, **21**, 6924–6936.